Research Square

Preprints are preliminary reports that have not undergone peer review.
They should not be considered conclusive, used to inform clinical practice,
or referenced by the media as validated information.

CCR2-dependent recruitment of SPP1+ macrophages promoted noise-induced hearing loss via pyroptosis

Ziqi wu
Air Force Medical University
Xinyuan zhang
Air Force Medical University
Meihao qi
Air Force Medical University
Xinyv dong
Air Force Medical University
Zejun gao
Air Force Medical University
Peng zhang
Air Force Medical University
Xinyv zhang
Air Force Medical University
Wenyue wang
Air Force Medical University
Renfeng wang
Air Force Medical University
Yang yang
Air Force Medical University
Bei fan
Air Force Medical University
Jun chen
Air Force Medical University
Xiaocheng wang
Air Force Medical University
Dingjun zha
zhadjun@fmmu.edu.cn

Air Force Medical University

Research Article

Keywords: Noise-induced hearing loss (NIHL), Macrophages, SPP1 (secreted phosphoprotein 1, Osteopontin), Pyroptosis, CCR2(C-C motif chemokine receptor 2)

Posted Date: August 14th, 2026

DOI: https://doi.org/10.21203/rs.3.rs-10588976/v1

License: This work is licensed under a Creative Commons Attribution 4.0 International License. Read Full License

Additional Declarations: No competing interests reported.

Abstract

Recent studies have highlighted the pivotal role of macrophages in the cochlea following acoustic stimulation. Here, we investigated the contribution of secreted phosphoprotein 1 (SPP1, osteopontin)-expressing macrophages to noise-induced hearing loss (NIHL). Single-cell RNA sequencing of murine cochleae revealed expansion of a macrophage subset characterized by high expression of Ccr2 and Spp1 at three days post-noise exposure. Genetic ablation of Ccr2 or Spp1 attenuated noise-induced auditory deficits. Cell–cell interaction analysis suggested that SPP1 enhances the phagocytic activity of $SPP1^+$ macrophages and promotes their recruitment to cochlear hair cells and neurons. Immunofluorescence staining and ELISA demonstrated that pyroptosis of $SPP1^+$ macrophages was associated with local inflammation and tissue damage. Pharmacological inhibition of SPP1 or CCR2 partially prevented noise-induced hearing loss. Collectively, these findings suggest that $SPP1^+$ macrophages may represent a potential therapeutic target for NIHL.

Introduction

Noise-induced hearing loss (NIHL) represents a major public health burden worldwide, with an estimated 1.1 billion young individuals at risk of preventable hearing loss due to recreational noise exposure[1]. Despite advances in understanding cochlear pathophysiology, no Food and Drug Administration-approved pharmacologic therapies currently exist for NIHL, reflecting the complexity of its underlying mechanisms and the lack of clearly defined therapeutic targets[2] [3]

The cochlea was conventionally regarded as an immune-privileged organ[4, 5] However, a growing body of evidence in recent years has verified that macrophages exert critical roles upon cochlear stimulation[6-8]. Under homeostatic conditions, resident macrophages of the murine cochlea, also referred to as microglia, originate from the yolk sac or liver and are involved in synaptic pruning and tissue regression during normal development[9]. Following noise exposure, substantial macrophage recruitment occurs in the cochlea[10, 11], with these cells appearing near the organ of Corti, a region devoid of macrophages under steady-state conditions. This dynamic response suggests that infiltrating or expanded macrophage populations may adopt specialized functions in the injured cochlea. Immune cell activation, particularly of macrophages, has emerged as a key determinant of cochlear injury and repair following acoustic overstimulation[12-14]. However, the functional heterogeneity of cochlear macrophages and the molecular drivers of their phenotypic transitions in response to noise remain incompletely understood.

Recent single-cell transcriptomic studies have begun to unravel the cell-type-specific landscape of the cochlea, including the diversity of cochlear immune cells following noise exposure[15, 16]. In the context of acoustic trauma, macrophages have been shown to exhibit distinct activation states and spatial distribution patterns[7]. Notably, secreted phosphoprotein 1 (SPP1, also known as osteopontin) has been implicated in various inflammatory and tissue remodeling processes across multiple organ systems[17-19]. In the inner ear, proteomic analyses have identified SPP1 as a component of the endolymph,

suggesting its potential involvement in cochlear homeostasis[20]. Furthermore, SPP1-expressing macrophages have been implicated in various pathological contexts, including age-related hearing loss, where elevated SPP1 expression has been observed in the cochlea and auditory cortex[21]. Whether SPP1⁺ macrophages play a similarly pivotal role in the cochlear response to noise injury remains to be elucidated.

CCR2 is a well-established marker for monocyte-derived macrophages and plays a critical role in mediating their recruitment from the circulation to sites of inflammation[22-24]. In various disease models, including atherosclerosis and atrial fibrillation, CCR2 signaling has been shown to drive the accumulation of pro-inflammatory macrophages that exacerbate tissue injury[22, 23]. However, the contribution of CCR2-mediated macrophage recruitment to cochlear pathology following noise exposure remains poorly defined.

In this study, we investigated the temporal dynamics, origin, and functional contributions of SPP1⁺ macrophages in a mouse model of NIHL. By integrating single-cell RNA sequencing, genetic knockout models, pharmacological inhibition, and functional assays, we sought to determine whether SPP1⁺ macrophages represent a pathogenic subset that drives cochlear inflammation and hearing loss. Our findings suggest that SPP1⁺ macrophages may represent a potential therapeutic target for NIHL and provide mechanistic insights into the interplay between macrophage phagocytosis, pyroptosis, and cochlear damage following acoustic overstimulation.

Results

We analyzed a publicly available scRNA-seq dataset of cochlear immune cells (*12)* following noise exposure, originally generated from mice at baseline (pre-noise) and at 3, 7, and 14 days after exposure to 105 dB broadband white noise for 2 hours. After quality control filtering (nFeature_RNA > 500 and < 6,000, nCount_RNA < 40,000, percent.mt < 7%), 1,556 cells were initially retained. Following doublet removal, 1,258 high-quality immune cells were obtained for downstream analysis. These cells were clustered into 12 distinct groups and annotated using established lineage markers, yielding populations of 596 neutrophils, 379 B cells, 187 T cells, and 96 macrophages (Fig 1A, B).

We observed a distinct temporal distribution pattern of cochlear macrophages following noise exposure. At three days post-noise (3dNE), the number of macrophages nearly doubled compared to baseline (pre-noise). In contrast, macrophage numbers at both 7 and 14 days post-noise were less than half of baseline levels (Fig 1C). Dimensionality reduction revealed that macrophages segregated into two distinct clusters, designated Cluster 10 and Cluster 11 (Fig 1A, B). Notably, macrophages from the 3dNE samples were predominantly localized to Cluster 11, whereas those from other time points were mostly distributed within Cluster 10 (Fig 1C). This time-restricted clustering suggests that macrophages at 3dNE may represent a functionally distinct subpopulation, warranting further investigation.

Differential gene enrichment analysis revealed that phagocytosis and pyroptosis

related pathways were significantly upregulated in the SPP1-expressing macrophage cluster.

To explore the functional differences between these two macrophage clusters, we performed differential gene expression analysis between Cluster 10 and Cluster 11 macrophages. Gene Set Enrichment Analysis (GSEA) of Kyoto Encyclopedia of Genes and Genomes (KEGG) pathways revealed that Cluster 11 macrophages exhibited significant enrichment of gene sets associated with lysosomal activation, efferocytosis (phagocytic clearance of apoptotic cells), Staphylococcus aureus infection, and monocyte recruitment (Fig 1.D).

Among the top 20 differentially expressed genes (DEGs) between Cluster 10 and Cluster 11 macrophages, the most highly expressed genes included C1qa, C1qb, C1qc, Trem2, SPP1, and Apoe (Fig 1.F). Additionally, MS4A7 was identified among the highly expressed genes in this cluster. Further analysis revealed significant upregulation of Il1b and Nlrp3 expression levels in macrophages following noise exposure (Fig 1H). Moreover, IL-1β expression differed markedly between $Spp1^{+}$ and $Spp1^{-}$ macrophage subsets (Fig 1I).

Through analysis of publicly available single-cell datasets derived from human inner ear and vestibular tissues[25], we identified the presence of $SPP1^{+}$ macrophages in the human inner ear, with significant correlations in gene expression profiles compared to their murine counterparts (Fig S1F). Gene Set Enrichment Analysis (GSEA) of expressed genes in both species revealed that $SPP1^{+}$ macrophages in humans and mice share enrichment of pathways related to response to peptides, inflammatory cytokine activation, and pro-inflammatory and pro-fibrotic processes (Fig S1C–E).

SPP1 expression in the cochlea and macrophages at selected time points following noise exposure

Based on our sequencing results, we hypothesized the existence of a specialized macrophage subpopulation characterized by high SPP1 expression following noise exposure and further speculated that this subpopulation may contribute to the pathology of noise-induced hearing loss (NIHL).

To investigate the presence of $SPP1^{+}$ macrophages in the cochlea after noise exposure, we exposed C57BL/6 mice to 110 dB broadband white noise to establish a NIHL model[26, 27], following our laboratory's established experimental framework. Auditory assessments revealed permanent threshold shifts in auditory brainstem response (ABR) at 14 days post-noise exposure (Fig S2 C). Histological analysis confirmed irreversible damage, including significant loss of hair cells and ribbon synapses (Fig S2 A and B).

Western blot analysis demonstrated a 1.7-fold increase in cochlear SPP1 protein levels at 3 days post-noise compared to baseline (Fig 2 E and F). Immunofluorescence staining of cochlear basilar membrane whole mounts at baseline and at 1, 3, and 14 days post-noise (Fig 2A) confirmed the presence of $SPP1^{+}$ macrophages, which were predominantly localized around the hair cell region. The density of $SPP1^{+}$ macrophages was quantified as 2–4 cells per 100 μm at 1 day and 3–5 cells per 100 μm at 3 days post-noise. In contrast, virtually no $SPP1^{+}$ macrophages were detected in the apical, middle, or basal turns of

control cochleae or at 14 days post-noise (Fig 2B). Ultrastructural analysis revealed that macrophages in the basilar membrane of wild-type mice at 3 days post-noise exhibited pronounced membrane protrusions and an increased number of lysosomes compared to the pre-noise state (Fig 2D). Collectively, these findings support the presence of a distinct SPP1$^+$ macrophage subpopulation in the cochlea at 3 days post-noise exposure.

Furthermore, we observed markedly elevated SPP1 immunoreactivity in supporting cells, the spiral ligament, and nerve fiber regions of cochlear whole-mount preparations at 3 days post-noise . This observation suggests that macrophages are not the exclusive source of SPP1 in the noise-exposed cochlea.

To explore the potential relevance of SPP1$^+$ macrophages to human pathophysiology, we analyzed publicly available single-cell datasets derived from human inner ear specimens. Our analysis revealed the presence of macrophages expressing SPP1 in both adult vestibular and fetal inner ear samples. Comparative pathway enrichment analysis between human SPP1$^+$ macrophages and their murine counterparts showed a positive correlation in gene expression profiles (R = 0.22, P = 0.00013) (Fig S1 F).

CCR2 signaling mediates the recruitment of SPP1$^+$ macrophages after noise exposure

We analyzed the expression of *Ccr2* and *P2ry12* in the noise-exposed cochlear SPP1$^+$ macrophage subpopulation from our sequencing data. The results showed that more than 80% of macrophages with high *SPP1* expression were CCR2-positive, whereas macrophages highly expressing the microglial marker P2RY12 were predominantly SPP1-negative (Fig S4 B).

We performed flow cytometry on peripheral blood from mice at various time points after noise exposure, using CD11b and F4/80 to label monocyte/macrophage-like cells. The proportion of these cells in the blood increased significantly as early as 1 h post-noise, peaked at 12 hours, and returned to near-baseline levels by day 1. Notably, the proportion of SPP1 and CCR2 double-positive cells increased markedly at 1 h post-noise and normalized by 12 hours (Fig 3A–C). To investigate whether SPP1$^+$ macrophages arise from local proliferation of resident cochlear macrophages, we performed Ki67 staining on cochlear basilar membranes after noise exposure.

To further explore the role of CCR2 signaling following noise exposure, we subjected C57BL/6 background CCR2 knockout (*Ccr2* $^{KO/KO}$) mice to noise. *Ccr2* $^{KO/KO}$ mice exhibited normal baseline hearing (Fig S3B). At 14 days post-noise, compared to wild-type mice, *Ccr2*$^{KO/KO}$ mice showed reduced ABR threshold shifts (Fig 7B), a significantly higher number of surviving synapses (Fig 7D, E), and increased outer hair cell survival in the basal turn (Fig 7A, C). To assess the impact on SPP1$^+$ macrophage abundance, we dissociated cochlear tissues from naive wild-type mice, noise-exposed wild-type mice, and noise-exposed *Ccr2* $^{KO/KO}$ mice at 3 days post-exposure. Immune cells were isolated using magnetic bead sorting and subjected to single-cell RNA sequencing. The results demonstrated that CCR2 knockout led to a reduction in the total number of cochlear immune cells (Fig 4B) and a decrease in the SPP1$^+$ macrophage population (Fig 4C) at 3 days post-noise. Immunofluorescence

staining of cochlear basilar membranes further confirmed a significant reduction in the number of SPP1^{+} macrophages surrounding hair cells in *Ccr2* $^{KO/KO}$ mice (Fig 4D, E). We performed clustering and differential gene analysis on macrophages before and after noise exposure, which further confirmed that the microglial subset (P2y12+) did not express Spp1, and Spp1^{+} macrophages showed no significant expression of proliferation-related genes after noise. In addition, we found that the proliferating macrophage subset (Mki67+) expressed Ccr2.

Frequent predicted cell–cell communication of SPP1^{+} macrophages after noise exposure

CellChat analysis predicted that SPP1^{+} macrophages exhibited the most extensive cell–cell communication network after noise exposure (Fig 5 B). Notably, SPP1^{+} macrophages were predicted to interact with nearly all other cell types analyzed (Fig 5 C).

The analysis further identified that macrophages may engage in communication through SPP1 interacting with two integrin pairs, CD44 and ITGAV+ITGB1. These predicted interactions were implicated in signaling to supporting cells, hair cells, and neurons, as well as in the regulation of macrophages, B cells, T cells, and neutrophils (Fig 5D).

Decreased expression of phagocytosis- and proinflammation-associated molecules in macrophages of *Spp1* $^{KO/KO}$ mice after noise exposure

Analysis of ligand-receptor expression changes in macrophages before and after noise exposure revealed upregulation of molecules associated with a pro-inflammatory macrophage state, including *Lgals9*[28, 29], *Fn1*[30-32], and *Mif* [33, 34]. (Fig 5 G) Macrophages also exhibited high expression of receptors such as *Cd44*, *Ccr2*, and *Tyrobp*. (Fig 5 I)

In *Spp1* $^{KO/KO}$ mice, the expression levels of *Lgals9*, *Fn1*, and *Mif* were reduced (Fig 5 F). The expression of macrophage receptors *Ccr2* and *Tyrobp* was also decreased (Fig 5 H). *Tyrobp* expression levels increased after noise exposure, along with an increase in the proportion of macrophages expressing it. While *Spp1* knockout led to a decrease in overall *Tyrobp* expression level, the proportion of macrophages expressing *Tyrobp* further increased.

We found that the overall *Trem2* expression level in macrophages decreased after noise exposure (Fig 5H) and was partially restored in *Spp1* $^{KO/KO}$ mice (Fig 5H). Our prior sequencing results indicated that the SPP1^{+} macrophage subpopulation is enriched in pathways related to efferocytosis (Fig 1F).

Collectively, these observations suggest that SPP1 may be involved in regulating the expression of pro-inflammatory and pro-fibrotic molecules in cochlear macrophages after noise exposure, although the underlying mechanisms remain to be further investigated.

The levels of pyroptosis-related inflammatory factors are downregulated in SPP1-knockout mice following noise exposure

Single-cell sequencing analysis revealed an increased proportion of macrophages expressing cell death molecules after noise exposure (Fig 6 A -D), and *Spp1* knockout resulted in a reduced proportion of pyroptosis macrophages. Knockout of *spp1* reduced the proportion of macrophages expressing the pyroptosis-related molecules caspase-1 and caspase-4, whereas the proportion of apoptotic molecules expressed in macrophages was not affected by *spp1* knockout.

ELISA analysis of cochlear protein lysates showed that IL-1β and IL-18 levels were elevated after noise exposure in wild-type mice, whereas this increase was attenuated in *Spp1* $^{KO/KO}$ mice（Fig 6 J-L）. We analyzed key molecules involved in the pyroptosis pathway [35-37]and found that *spp1* knockout had no significant effect on the proportion of macrophages expressing Nlrp3, GSDMD, and IL-1β. Only the proportion of caspase-1^{+} macrophages was markedly decreased after *spp1* deletion under noise exposure conditions. （Fig 6 E-I）

Collectively, these observations suggest that SPP1 may be associated with enhanced pyroptosis-related inflammatory responses in cochlear macrophages after noise exposure, although direct causal evidence remains to be established.

SPP1 and CCR2 inhibition attenuates noise-induced hearing loss

To evaluate the potential of targeting SPP1^{+} macrophages in NIHL, we used pharmacological inhibitors against SPP1 and CCR2, as well as two transgenic mouse lines: *Ccr2* $^{KO/KO}$ and *Spp1* $^{KO/KO}$ mice. Baseline auditory function, assessed by ABR thresholds across frequencies, showed no significant differences between knockout and WT mice before noise exposure (Fig S3B). Immunofluorescence staining confirmed that hair cell and synapse counts in knockout mice were comparable to those in WT controls under baseline conditions (Fig S3A, C–E).

We then exposed WT, *Spp1* $^{KO/KO}$, and *Ccr2* $^{KO/KO}$ mice to 110 dB broadband noise. At 14 days post-exposure, both *Spp1* $^{KO/KO}$ and *Ccr2* $^{KO/KO}$ mice exhibited reduced ABR threshold shifts compared to WT mice. Immunofluorescence analysis of cochlear basilar membranes revealed that *Ccr2* $^{KO/KO}$ mice retained more hair cells and synapses than WT controls after noise exposure.

In parallel, we administered SPP1 and CCR2 inhibitors via intraperitoneal injection to WT mice, with a control group receiving saline (Fig 8A). At 14 days post-noise, ABR threshold shifts were attenuated in both inhibitor-treated groups relative to the saline control (Fig 8B). Consistent with the genetic knockout findings, inhibitor-treated mice also showed enhanced preservation of hair cells and synapses (Fig 8C–F). Collectively, these observations suggest that targeting SPP1 or CCR2 may attenuate noise-induced hearing loss and cochlear damage.

Discussion

In this study, we identified a distinct SPP1^{+} macrophage subpopulation that expands in the cochlea at three days post-noise exposure and contributes to noise-induced hearing loss (NIHL) pathology. Through

integrated single-cell RNA sequencing, genetic knockout models, and pharmacological inhibition, we demonstrated that these macrophages are predominantly derived from CCR2$^+$ peripheral monocytes and recruited to the cochlea following acoustic overstimulation. Functionally, SPP1$^+$ macrophages exhibit pro-inflammatory and pro-fibrotic properties, as evidenced by upregulated pathways and molecules in single-cell RNA sequencing data, including Spp1, Fn1 and Il-1β. This pro-inflammatory state was accompanied by increased expression of pyroptosis-associated markers, including NLRP3, IL-1β, IL-18, and Caspase-1, which were attenuated in *Spp1*-deficient mice. Genetic ablation or pharmacological inhibition of SPP1 or CCR2 significantly reduced noise-induced auditory threshold shifts and preserved cochlear hair cells and ribbon synapses. Collectively, these findings suggest that the SPP1-CCR2 axis orchestrates the recruitment and pro-inflammatory activation of a pathogenic macrophage subset, positioning SPP1$^+$ macrophages as a potential therapeutic target for NIHL, pending further validation.

While SPP1 has been detected in endolymph under steady-state conditions[20], our findings suggest its upregulation in macrophages and supporting cells following acoustic trauma, raising the possibility of a context-dependent functional shift. Elevated SPP1 expression has also been reported in age-related hearing loss[21], implying a potential role across different forms of hearing impairment. Building on a previous transcriptomic atlas[15], our study provides preliminary insights into a potential pathogenic SPP1$^+$ macrophage subset and its recruitment in NIHL, pending further mechanistic validation.

The gene signature observed in the SPP1$^+$ macrophage cluster, including *C1qa*, *C1qb*, *C1qc*, *Trem2*, *SPP1*, and *Apoe*, has been previously characterized as a disease-associated module[38]. In Alzheimer's disease models, SPP1 secreted by perivascular macrophages and fibroblasts mediates microglial phagocytosis of ApoE-labeled synaptic structures, a process in which complement component C1q plays a critical role[39]. Additionally, *MS4A7*, which was highly expressed in this cluster, has been reported to directly activate the NLRP3 inflammasome in macrophages, thereby exacerbating local inflammatory responses[40, 41]. The upregulation of *Il1b* and *Nlrp3* in macrophages after noise exposure, together with the differential IL-1β expression between Spp1$^+$ and Spp1$^-$ subsets, suggests that the Spp1$^+$ macrophage subpopulation may be involved in modulating pyroptosis-related pathways and may exert pro-inflammatory functions in response to noise, although this possibility requires further functional validation.

The origin of cochlear macrophages after noise exposure remains debated. Macrophage function and differentiation are closely linked to their origins[42]. Resident macrophages in homeostatic tissues typically exert anti-inflammatory functions, whereas recruited macrophages contribute to disease pathology in conditions such as myocardial infarction and stroke[43]. CCR2 is recognized as a marker for monocyte-derived macrophages[22, 23, 44], while P2RY12 serves as a stable marker for microglia[45, 46]. Our observation that SPP1$^+$ macrophages are predominantly CCR2$^+$ and negative for P2RY12, together with the absence of Ki67 positivity, raises the possibility that these cells originate from peripheral monocytes rather than local proliferation. Using Ccr2RFP/+ Cx3cr1GFP/+ dual-reporter mice, Pan et al.[7] reported that tissue-resident macrophages dominate the cochlear response to noise and contribute to hair cell damage. In contrast, our findings suggest that the expanded SPP1$^+$ macrophage

population is predominantly derived from CCR2^{+} peripheral monocytes. This discrepancy may reflect differences in noise exposure paradigms, mouse strains, or the specific macrophage subsets analyzed. Our observation that CCR2 knockout reduces both the number of SPP1^{+} macrophages and noise-induced hearing loss further supports a functional role for monocyte-derived macrophages in NIHL pathology, consistent with studies implicating CCR2 signaling in monocyte recruitment across various inflammatory conditions[23, 43, 47].

CellChat analysis predicted that SPP1⁺ macrophages serve as a central hub in the cochlear cell–cell communication network after noise exposure, with predicted interactions involving SPP1-CD44 and SPP1-ITGAV+ITGB1 signaling axes. These predictions are consistent with findings in other pathological contexts. For instance, SPP1⁺ tumor-associated macrophages have been shown to remodel the tumor microenvironment through SPP1-CD44 interactions[48], and perivascular SPP1 signaling has been demonstrated to induce microglial phagocytosis in Alzheimer's disease models[39]. Moreover, SPP1^{+} macrophages have been shown to define a distinct macrophage polarity that coordinates cellular programs across multiple cell types in the tumor microenvironment, influencing disease progression and patient outcomes[49]. Collectively, these observations suggest that SPP1^{+} macrophages may play a conserved role in orchestrating intercellular communication across diverse inflammatory conditions, including NIHL.

We found that the expression of pyroptosis-related markers, including Caspase-1, IL-1β and IL-18, was increased after noise exposure, and these markers were attenuated in Spp1-deficient mice. This finding raises the possibility that Spp1 is associated with inflammatory cell death of cochlear macrophages. Similar associations between disease and pyroptosis have been observed in other contexts[50-52], leading us to propose that Spp1 induces macrophages to undergo pyroptosis in the cochlea, and the subsequent release of inflammatory factors leads to tissue inflammation and fibrosis.

Similar links between phagocytosis and pyroptosis have been reported in other contexts, where excessive efferocytosis triggers caspase-dependent pyroptosis and IL-1β maturation[53]. NLRP3 inflammasome activation in cochlear macrophages has also been implicated in NIHL and other auditory pathologies[7, 53, 54], supporting a pathogenic role for macrophage inflammasome activation. We also observed that SPP1 deficiency reduced pro-inflammatory molecules (*Lgals9*, *Fn1*, *Mif*) and the recruitment-associated receptor *Ccr2* in cochlear macrophages after noise exposure, raising the possibility that SPP1 may influence macrophage phenotypic transition. Consistent with this, *Trem2*, a key immune surveillance molecule[7, 55], was downregulated after noise exposure and partially restored in *Spp1*$^{KO/KO}$ mice, suggesting SPP1 may be involved in the homeostatic to pro-inflammatory shift. Our finding that *Tyrobp*, a phagocytosis-associated adaptor that forms a signaling complex with TREM2, was differentially regulated after *Spp1* knockout suggests a potential interplay between SPP1 and TYROBP signaling in cochlear macrophages. This is consistent with a previous study showing that long-term running exercise upregulates both SPP1 and TYROBP expression in the hippocampus of APP/PS1 mice, accompanied by enhanced microglial metabolic activity and morphological plasticity[56].

Finally, our findings show that genetic ablation or pharmacological inhibition of SPP1 and CCR2 attenuates noise-induced hearing loss and cochlear damage, supporting a functional role for these molecules in NIHL. The protective effects observed in *Ccr2*$^{KO/KO}$ mice are consistent with the established role of CCR2 in monocyte recruitment across inflammatory conditions[23, 43, 57]. The therapeutic potential of targeting macrophages in hearing loss is supported by recent studies showing that pyroptosis enhances macrophage phagocytic activity[58] [59]and that inhibiting TLR4 signaling in cochlear macrophages alleviates noise-induced damage[7]. These findings, together with our results, suggest that modulating macrophage function may represent a viable strategy for treating auditory injury.

Several limitations should be acknowledged. First, the use of systemic knockout and pharmacological inhibitors does not allow for cell-type-specific conclusions; conditional knockout models are needed to validate the macrophage-intrinsic roles of SPP1 and CCR2. Second, CellChat predictions of ligand-receptor interactions require experimental validation, such as through neutralizing antibodies or genetic disruption. Third, direct evidence of macrophage pyroptosis, including cleaved GSDMD or ASC speck formation, is lacking. Fourth, the scRNA-seq dataset (105 dB) and functional experiments (110 dB) used different noise paradigms, warranting cautious interpretation when integrating these datasets. Addressing these limitations will help solidify the mechanistic understanding of SPP1^{+} macrophages in NIHL.

Material and method

Animal

All C57BL/6J mice used in this study were obtained from the Laboratory Animal Center of Air Force Medical University. SPP1$^{KO/KO}$ mice on a C57BL/6J background were generated by Cyagen Biosciences (Suzhou, China). CCR2$^{KO/KO}$ mice were purchased from Cyagen Biosciences (Suzhou, China). All experimental procedures were approved by the Institutional Animal Care and Use Committee (IACUC) of Air Force Medical University (Protocol No. IACUC-20260039) and were conducted in accordance with the National Institutes of Health (NIH) Guide for the Care and Use of Laboratory Animals. Every effort was made to minimize the number of animals used and to reduce potential suffering. Euthanasia of postnatal and adult mice was performed under deep anesthesia with sodium pentobarbital, following the American Veterinary Medical Association (AVMA) Guidelines for the Euthanasia of Animals (2020 Edition). For mice that underwent auditory brainstem response (ABR) testing, cochleae were collected immediately after the assessment via cervical dislocation under sustained anesthesia.

Noise Exposure

Six-week-old mice were individually placed in cages (9 cm in diameter) and exposed to a 110 dB SPL broadband noise (2–20 kHz) for 2 hours. The noise exposure was conducted within a dedicated sound chamber equipped with a loudspeaker (Model 2450H, JBL, Los Angeles, CA, USA) driven by a power amplifier (AX-500U, Yamaha, Maebashi, Japan). To ensure uniformity of the noise exposure, the sound

pressure level was calibrated and verified at multiple positions inside the chamber using a sound level meter (TES 1350A, Taiwan, China).

Single-cell isolation

The organ of Corti, lateral wall, spiral ganglion, and modiolus were dissected from mouse cochleae and digested with papain (20 U/mL; Worthington) in HBSS containing 1 mM L-cysteine and 0.5 mM EDTA for 20 min at 37°C. After gentle trituration, the suspension was filtered through a 40 μm strainer. Total immune cells were isolated using CD45 MicroBeads (Miltenyi Biotec,130-052-301) according to the manufacturer's protocol. $CD45^{+}$ cells were eluted and counted before downstream analysis.

Single-cell RNA sequencing (scRNA-seq) analysis

Designated cells were sorted into PBS following the 10× Genomics protocol. The resulting cell suspension was loaded into a Chromium Controller (10x Genomics), and single-cell cDNA libraries were then constructed using Chromium Single Cell 3' Reagent kits (v3) following the manufacturer's protocols. The libraries were quantified and subjected to 150 bp paired-end sequencing on an Illumina NovaSeq 6000 platform (Illumina).

Raw base call files were demultiplexed using the 10x Genomics Cell Ranger pipeline and aligned to the mice transcriptome. Raw gene expression matrices were imported into R (version 4.1.2). Seurat package was used for cell filtration, normalization of data, reduction of dimensionality reduction, cell cluster, and differentially expressed gene identified. Cells with less than 200 genes and more than 5000 genes or mitochondrial genes of more than 10 were excluded for subsequent data analysis. 'FindVariableFeatures' was used to identify the top 2000 most hypervariable genes, and these genes were selected for principal component analysis (PCA) and linear dimension reduction. The original Louvain algorithm (FindClusters) with a clustering resolution of 0.6 was performed to cluster the cells. Differentially expressed genes of each sample were conducted using a Wilcoxon rank-sum test with p-value < 0.05, log(fc.threshold) =0.25. Cell types were allocated to each cluster using the known marker genes as described previously

To explore the potential mechanisms by which SPP1 signaling may contribute to hearing loss, we generated *Spp1*$^{KO/KO}$ mice on a C57BL/6 background. Following the same experimental protocol, immune cells were isolated and subjected to single-cell RNA sequencing. The resulting immune cell data were then integrated and normalized with previously published single-cell datasets from supporting cells, spiral ganglion neurons, and hair cells under both pre- and post-noise conditions (Dataset 1). This combined dataset was used for dimensionality reduction analysis and subsequent CellChat analysis to predict cell–cell communication patterns.

Auditory Brainstem Response (ABR) Measurement

Mice were anesthetized via intraperitoneal injection of sodium pentobarbital (50 mg kg^{-1}) and placed on a temperature-controlled heating pad within a sound-attenuating, electrically shielded chamber.

Frequency-specific auditory responses were recorded using a Tucker-Davis Technologies (TDT, Alachua, FL, USA) RZ6 system. Subdermal needle electrodes were positioned at the vertex (midline suture), ipsilateral mastoid region, and tail base (ground). Acoustic stimuli (15 ms tone bursts with 1 ms rise/fall time) were generated, and responses were recorded using TDT System III hardware and SigGen/Biosig software. The ABR signals were filtered (high-pass: 300 Hz; low-pass: 3 kHz). Hearing thresholds were determined at 8, 16, 24, and 32 kHz by initially decreasing stimulus intensity in 10-dB steps and then in 5-dB steps near the threshold until a reproducible waveform was no longer detectable. The threshold was defined as the lowest stimulus intensity level at which a distinct, repeatable wave pattern could be visually identified. All ABR measurements were performed by a single experienced experimenter, and threshold determinations were made by an expert who was blinded to the experimental conditions.

Immunofluorescence staining

The cochlear of the mice treated as described above were removed and fixed with 4% paraformaldehyde at 4 °C for 12 h. After decalcification by soaking in 10% EDTA, the basilar membrane was removed. After being washed with 1× PBS (Cytiva; SH30256.01), the cells were treated with 0.5%-1% Triton X-100 (Biosharp, BS084) at room temperature for 10 min and blocked with 5% BSA at 37 °C for 45 min. Primary antibodies were diluted with an antibody diluent. Fifty microliters of diluted antibodies were added to each cochlear tissue sample. After incubation at 4 °C for 48 h, the samples were washed with 1 × PBS, a fluorescent secondary antibody was added, the samples were wrapped with tin foil in the dark, incubated at room temperature for 24 h, rinsed with 1× PBS, and incubated with DAPI (1:1000; Sigma; 28718-90-3) or phalloidin (1:200; Abcam; ab176753). After the samples were washed, they were placed on a slide and observed under a laser confocal microscope. ImageJ (Fiji; 1.54d) was used to perform a semiquantitative analysis of the laser confocal images. The following primary antibodies were used: rabbit polyclonal anti-myosin 7a (1:1000; Proteus Biosciences; 25-6790), goat polyclonal anti-SPP1 (1 μg/mL; R&D Systems; AF808-SP), mouse monoclonal anti-Iba1 (1:800; ASIS; OB-IF-Fr-HH01), rabbit polyclonal anti-Iba1 (1:200; Affinity; DF6442), mouse monoclonal anti-CtBP2 (1:200; BD Biosciences; 612044), rabbit polyclonal anti-CD68 (1:200; Affinity; DF7518). Secondary antibodies (1:400; D-R; 647;Invitrogen; A31573), (1:400; D-R; 594 Invitrogen;A21207) , (1:400; D-R; 488 Invitrogen; A21206) , (1:400; D-G; 594 Invitrogen; A11058) , (1:400; D-M; 594 Invitrogen; A11005), (1:400; D-M; 488 Invitrogen; A32766) were used for detection.

Western Blotting

The cochlear tissue was placed in RIPA lysis buffer (Glpbio; GK10023) containing PMSF (1:100; Glpbio; GC10477) and a protease inhibitor cocktail (1:100; Glpbio; GK10014). The protein concentration was measured using a BCA protein assay kit (Glpbio; GK10009). A total of 30 μg of each protein sample was separated on 4–12% SDS–PAGE gels. After electrophoresis, the proteins were transferred to a polyvinylidene difluoride membrane. The membrane was incubated with a primary antibody overnight at 4 °C and then with a secondary antibody at 37 °C for 1 h. After three washes, the bands were visualized via a chemiluminescence substrate (Millipore, WBKLS0500) and analyzed using ImageJ software. The

following primary antibodies were used: goat polyclonal anti-spp1 (0.1ug/ml; R□D; AF808-SP), and mouse monoclonal anti-β-Actin (1:1000; Abcam; ab8226). The following secondary antibody were used: HRP-conjugated AffinityPure goat anti-rabbit (or anti-mouse) IgG (1:5000, Proteintech, SA00001-2, SA00001-1), HRP-conjugated rabbit anti-goat(affinity;1:10000). Each experiment was repeated more than 3 times.

Flow Cytometry and Cell Sorting

Fresh anticoagulated blood was centrifuged at 400-500 ×g for 5 minutes, and the supernatant was discarded. The cell pellet was resuspended in 6-10 volumes of red blood cell (RBC) lysis buffer, gently mixed, and incubated at room temperature for 1-2 minutes. Following lysis, the sample was centrifuged again (400-500 ×g, 5 minutes), and the red supernatant was discarded. This lysis step was repeated once. The remaining cells were washed twice with 5 ml phosphate-buffered saline (PBS) to obtain the final cell suspension for analysis.

The cell pellet was divided into two aliquots. One aliquot was used for cell counting. The other was stained for flow cytometry. First, cells were incubated with an Fc receptor blocking reagent for 10 minutes at room temperature. Subsequently, the following fluorochrome-conjugated antibodies were added and incubated for 30 minutes at 4°C in the dark: anti-CCR2 (3 μL; Biolegend, Cat# 150627), anti-CD11b (2 μL; Biolegend, Cat# 101229), and anti-F4/80 (2 μL; Biolegend, Cat# 111603). After staining, cells were resuspended in 1 mL of flow cytometry staining buffer, centrifuged, and the supernatant was discarded. For intracellular staining of SPP1, cells were fixed and permeabilized using the FIX & PERM™ Cell Permeabilization Kit (Thermo Fisher Scientific). Briefly, 100 μL of Medium A (fixation reagent) was added, cells were gently resuspended, and incubated for 20 minutes at room temperature in the dark. Cells were then washed with 1 mL of staining buffer and centrifuged. Next, 100 μL of Medium B (permeabilization reagent) and 1 μL of anti-SPP1 antibody (Sanying Biotechnology, Wuhan, China, Cat# cl488-22952) were added, followed by incubation for 30 minutes at room temperature in the dark. Finally, cells were washed with 1 mL of staining buffer and centrifuged. Stained samples were analyzed on a flow cytometer. Data processing and graphical representation were performed using FlowJo software (version 10.8.1).

Enzyme-linked immunosorbent assay (ELISA)

Cochlear tissues were collected and homogenized in ice-cold saline (9 volumes per gram of tissue) to prepare 10% (w/v) tissue homogenates. The homogenates were centrifuged at 2500–3000 rpm for 10 min at 4°C, and the supernatants were collected for subsequent analysis. Concentrations of IL-1β, IL-6, and IL-18 were measured using commercially available ELISA kits according to the manufacturers' protocols (IL-1β: EK201B, Lianke Bio; IL-6: EK206, Lianke Bio; IL-18: EK218, Lianke Bio). Absorbance was read at 450 nm using a microplate reader, and cytokine levels were calculated based on standard curves.

Drug Administration

For the SPP1 inhibitor group, C57BL/6 mice received a single intraperitoneal injection of an SPP1 inhibitor (MCE, HY-146064) at a dose of 70 mg kg^{-1}, administered one day prior to noise exposure. For the CCR2 inhibitor group, C57BL/6 mice were administered a CCR2 inhibitor (MCE, HY-18611) via daily intraperitoneal injection at a dose of 100 mg kg^{-1} for 10 consecutive days, commencing 10 days before noise exposure. Both inhibitors were first dissolved in dimethyl sulfoxide (DMSO) to prepare stock solutions according to the manufacturer's instructions and were subsequently diluted in sterile physiological saline to obtain the final working concentrations. Mice in the normal control group were injected subcutaneously with an equivalent volume of sterile physiological saline.

Statistical analysis

All data were analyzed using GraphPad Prism (version 9.0) and R software (version 4.5.2). Data are presented as mean ± standard error of the mean (SEM) unless otherwise indicated. Comparisons between two groups were performed using unpaired two-tailed Student's t-test. For comparisons involving more than two groups, one-way or two-way analysis of variance (ANOVA) was used, followed by Tukey's or Sidak's post hoc test for multiple comparisons, as appropriate. For auditory brainstem response (ABR) threshold shift analysis, two-way repeated measures ANOVA was applied to account for frequency and time factors.

For single-cell RNA sequencing data, differential gene expression analysis was performed using the Wilcoxon rank-sum test with a significance threshold of $p < 0.05$ and $\log_2$(fold change) threshold of 0.25. CellChat analysis was used to infer ligand-receptor interactions and cell-cell communication networks, with significance determined by permutation testing (1,000 permutations). For flow cytometry and immunofluorescence quantification, at least three independent biological replicates were analyzed per condition. Correlation analysis between gene expression profiles was assessed using Pearson's correlation coefficient.

All experiments were repeated at least three times independently unless otherwise specified. Statistical significance was defined as $p < 0.05$, with significance levels indicated as $^{*}p < 0.05$, $^{**}p < 0.01$, $^{***}p < 0.001$, and $^{****}p < 0.0001$. Blinding was applied during ABR threshold measurement and immunofluorescence image quantification to minimize bias.

Declarations

Acknowledgments: The authors thank (Wuhan Igenebook)Genome Sequencing Company for providing RNA-sequencing technical support and Cyagen (Suzhou) Biotechnology Company for generating Spp1KO/KO Ccr2 KO/KO mice.

Funding: This work was supported by the National Natural Science Foundation of China (82571312 to D.J.Z82301303 to B.F, 82401349 to Y.Y).

Author contributions: Z.Q.W performed the laboratory experiments. D.J.Z., J.C and X.C.W designed this study. X.Y.Z., M.H.Q., and P.Z. contributed to the mouse audiology tests. , Z.J.G., X.Y.Z,X.Y.D , and Q.Z.W. contributed to the data analysis. Z.Q.W., and X.Y.Z. contributed to the animal support for the study. Q.W. Z., and X.Y.Z. suggested changes to the figures. Z.Q.W., and , D.J.Z. and J.C contributed to critical discussions. Z.Q.W wrote the paper. All the authors read and approved the final manuscript.

Competing interests: The authors declare no conflict of interest.

Data and materials availability: The RNA-seq data are available in the GEO database under accession number GSE111413.

References

1. Chadha S, Kamenov K, Cieza A: **The world report on hearing, 2021.** *Bull World Health Organ* 2021, **99:**242-242A.
2. Feng B, Dong T, Song X, Zheng X, Jin C, Cheng Z, Liu Y, Zhang W, Wang X, Tao Y, Wu H: **Personalized Porous Gelatin Methacryloyl Sustained-Release Nicotinamide Protects Against Noise-Induced Hearing Loss.** 2024, **11:**2305682.
3. Xu K, Xu B, Gu J, Wang X, Yu D, Chen Y: **Intrinsic mechanism and pharmacologic treatments of noise-induced hearing loss.** *Theranostics* 2023, **13:**3524-3549.
4. Okano T, Nakagawa T, Kita T, Kada S, Yoshimoto M, Nakahata T, Ito J: **Bone marrow-derived cells expressing Iba1 are constitutively present as resident tissue macrophages in the mouse cochlea.** 2008, **86:**1758-1767.
5. Yang W, Vethanayagam RR, Dong Y, Cai Q, Hu BH: **Activation of the antigen presentation function of mononuclear phagocyte populations associated with the basilar membrane of the cochlea after acoustic overstimulation.** *Neuroscience* 2015, **303:**1-15.
6. Song X, Li Y, Guo R, Yu Q, Liu S, Teng Q, Chen ZR, Xie J, Gong S, Liu K: **Cochlear resident macrophage mediates development of ribbon synapses via CX3CR1/CX3CL1 axis.** *Front Mol Neurosci* 2022, **15:**1031278.
7. Pan J, Wang K, Qu J, Chen D, Chen A, You Y, Tang J, Zhang H: **Activated tissue-resident macrophages contribute to hair cell insults in noise-induced hearing loss in mice.** *Commun Biol* 2024, **7:**1078.
8. Sung CYW, Hayase N, Yuen PST, Lee J, Fernandez K, Hu X, Cheng H, Star RA, Warchol ME, Cunningham LL: **Macrophage depletion protects against cisplatin-induced ototoxicity and nephrotoxicity.** *Sci Adv* 2024, **10:**eadk9878.
9. Song X, Li Y, Guo R, Yu Q, Liu S, Teng Q, Chen Z-R, Xie J, Gong S, Liu K: **Cochlear resident macrophage mediates development of ribbon synapses via CX3CR1/CX3CL1 axis.** *Frontiers In Molecular Neuroscience* 2022, **15:**1031278.

10. Yi Y, Wu M-Y, Chen K-T, Chen A-H, Li L-Q, Xiong Q, Wang X-R, Lei W-B, Xiong G-X, Fang S-B: **LDHA-mediated glycolysis in stria vascularis endothelial cells regulates macrophages function through CX3CL1-CX3CR1 pathway in noise-induced oxidative stress.** *Cell Death & Disease* 2025, **16:**65.
11. Wu M-Y, Chen A-H, Li L-Q, Yi Y, Xiong Q, Chen K-T, Cai Z-M, Lei W-B, Xiong G-X, Fang S-B: **Single-cell RNA sequencing analysis of mouse cochlea identifies a novel proinflammatory CD74+CD14+ macrophage subset in mice with age-related and noise-induced hearing loss.** *Hearing Research* 2025, **466:**109376.
12. Pan J, Wang K, Qu J, Chen D, Chen A, You Y, Tang J, Zhang H: **Activated tissue-resident macrophages contribute to hair cell insults in noise-induced hearing loss in mice.** *Communications Biology* 2024, **7:**1078.
13. Song X, Li Y, Guo R, Yu Q, Liu S, Teng Q, Chen Z-R, Xie J, Gong S, Liu K: **Cochlear resident macrophage mediates development of ribbon synapses via CX3CR1/CX3CL1 axis.** 2022, **Volume 15 - 2022**.
14. Sung CYW, Hayase N, Yuen PST, Lee J, Fernandez K, Hu X, Cheng H, Star RA, Warchol ME, Cunningham LL: **Macrophage depletion protects against cisplatin-induced ototoxicity and nephrotoxicity.** 2024, **10:**eadk9878.
15. Milon B, Shulman ED, So KS, Cederroth CR, Lipford EL, Sperber M, Sellon JB, Sarlus H, Pregernig G, Shuster B, et al: **A cell-type-specific atlas of the inner ear transcriptional response to acoustic trauma.** *Cell Rep* 2021, **36:**109758.
16. Murali SV, Stothert AR, Pereyra E, Batalkina L, Kaur T: **CX3CR1 fate mapping in vivo distinguishes cochlear resident and recruited macrophages after acoustic trauma.** *Frontiers In Immunology* 2025, **16:**1678176.
17. Morse C, Tabib T, Sembrat J, Buschur KL, Bittar HT, Valenzi E, Jiang Y, Kass DJ, Gibson K, Chen W, et al: **Proliferating SPP1/MERTK-expressing macrophages in idiopathic pulmonary fibrosis.** *The European Respiratory Journal* 2019, **54**.
18. De Schepper S, Ge JZ, Sierksma A, Crowley G, Ferreira LSS, Garceau D, Toomey CE, Sokolova D, Rueda-Carrasco J, Shin S-H, et al: **Perivascular cells induce microglial phagocytic states and synaptic engulfment via SPP1 in mouse models of Alzheimer's disease.** *Nature Neuroscience* 2023, **26:**406-415.
19. Han H, Ge X, Komakula SSB, Desert R, Das S, Song Z, Chen W, Athavale D, Gaskell H, Lantvit D, et al: **Macrophage-derived Osteopontin (SPP1) Protects From Nonalcoholic Steatohepatitis.** *Gastroenterology* 2023, **165:**201-217.
20. Fukuda M, Okanishi H, Ino D, Ono K, Ota T, Wakai E, Sato T, Ohta Y, Kikkawa Y, Inohara H, et al: **Protein profile of mouse endolymph suggests a role in controlling cochlear homeostasis.** *iScience* 2024, **27:**111214.
21. Yuan Y, Zhang J, Zhao J, Zhang X, Cao Z: **Expression of ApoE and Spp1 in the cochlea and auditory cortex of age-related hearing loss mice.** *Braz J Otorhinolaryngol* 2025, **91:**101674.

22. Georgakis MK, Bernhagen J, Heitman LH, Weber C, Dichgans M: **Targeting the CCL2-CCR2 axis for atheroprotection.** *Eur Heart J* 2022, **43:**1799-1808.
23. Hulsmans M, Schloss MJ, Lee IH, Bapat A, Iwamoto Y, Vinegoni C, Paccalet A, Yamazoe M, Grune J, Pabel S, et al: **Recruited macrophages elicit atrial fibrillation.** *Science* 2023, **381:**231-239.
24. Al-Qazazi R, Lima PDA, Prisco SZ, Potus F, Dasgupta A, Chen K-H, Tian L, Bentley RET, Mewburn J, Martin AY, et al: **Macrophage-NLRP3 Activation Promotes Right Ventricle Failure in Pulmonary Arterial Hypertension.** *American Journal of Respiratory and Critical Care Medicine* 2022, **206:**608-624.
25. van der Valk WH, van Beelen ESA, Steinhart MR, Nist-Lund C, Osorio D, de Groot JCMJ, Sun L, van Benthem PPG, Koehler KR, Locher H: **A single-cell level comparison of human inner ear organoids with the human cochlea and vestibular organs.** *Cell Reports* 2023, **42:**112623.
26. Chen B, Sun Y, Sun H, Cong N, Ma R, Qian X, Lyu J, Fu X, Chi F, Li H, et al: **Ultrasound-Triggered NO Release to Promote Axonal Regeneration for Noise-Induced Hearing Loss Therapy.** *ACS Nano* 2024, **18:**33232-33244.
27. Qi M, Gao Z, Qiu Y, Wang R, Tian K, Yue B, Zhang X, Zhang P, Wu Z, Zhu Q, et al: **NOX2 Contributes to High-Frequency Outer Hair Cell Vulnerability in the Cochlea.** *Advanced Science (Weinheim, Baden-Wurttemberg, Germany)* 2025, **12:**e08830.
28. Li Y, Sang Y, Chang Y, Xu C, Lin Y, Zhang Y, Chiu PCN, Yeung WSB, Zhou H, Dong N, et al: **A Galectin-9-Driven CD11chigh Decidual Macrophage Subset Suppresses Uterine Vascular Remodeling in Preeclampsia.** *Circulation* 2024, **149:**1670-1688.
29. Fan G, Tao C, Li L, Xie T, Tang L, Han X, Shi Y: **The co-location of MARCO+ tumor-associated macrophages and CTSE+ tumor cells determined the poor prognosis in intrahepatic cholangiocarcinoma.** *Hepatology (Baltimore, Md)* 2024, **82:**25-41.
30. Ouyang Q, Wang C, Sang T, Tong Y, Zhang J, Chen Y, Wang X, Wu L, Wang X, Liu R, et al: **Depleting profibrotic macrophages using bioactivated in vivo assembly peptides ameliorates kidney fibrosis.** *Cellular & Molecular Immunology* 2024, **21:**826-841.
31. Hoeft K, Schaefer GJL, Kim H, Schumacher D, Bleckwehl T, Long Q, Klinkhammer BM, Peisker F, Koch L, Nagai J, et al: **Platelet-instructed SPP1+ macrophages drive myofibroblast activation in fibrosis in a CXCL4-dependent manner.** *Cell Reports* 2023, **42:**112131.
32. Wang J, Wang S, Ren L, Liu X, Zhang L, Hu P, Xu W, Zheng S, Liu J, Ling Q: **Targeting Itga8 Mitigates Neurogenic Bladder Fibrosis Driven by Trem2^{+} Macrophage-Derived Fn1 via FAK/RhoA/ROCK Signaling.** *Advanced Science (Weinheim, Baden-Wurttemberg, Germany)* 2025, **13:**e10631.
33. Sumaiya K, Langford D, Natarajaseenivasan K, Shanmughapriya S: **Macrophage migration inhibitory factor (MIF): A multifaceted cytokine regulated by genetic and physiological strategies.** *Pharmacology & Therapeutics* 2021, **233:**108024.
34. Zeng L, Hu P, Zhang Y, Li M, Zhao Y, Li S, Luo A: **Macrophage migration inhibitor factor (MIF): Potential role in cognitive impairment disorders.** *Cytokine & Growth Factor Reviews* 2024, **77:**67-75.

35. Yu P, Zhang X, Liu N, Tang L, Peng C, Chen X: **Pyroptosis: mechanisms and diseases.** *Signal Transduction and Targeted Therapy* 2021, **6:**128.
36. Liu Y, Pan R, Ouyang Y, Gu W, Xiao T, Yang H, Tang L, Wang H, Xiang B, Chen P: **Pyroptosis in health and disease: mechanisms, regulation and clinical perspective.** *Signal Transduction and Targeted Therapy* 2024, **9:**245.
37. Elias EE, Lyons B, Muruve DA: **Gasdermins and pyroptosis in the kidney.** *Nature Reviews Nephrology* 2023, **19:**337-350.
38. Li H, Miao Y, Zhong L, Feng S, Xu Y, Tang L, Wu C, Zhang X, Gu L, Diao H, et al: **Identification of TREM2-positive tumor-associated macrophages in esophageal squamous cell carcinoma: implication for poor prognosis and immunotherapy modulation.** *Front Immunol* 2023, **14:**1162032.
39. De Schepper S, Ge JZ, Sierksma A, Crowley G, Ferreira LSS, Garceau D, Toomey CE, Sokolova D, Rueda-Carrasco J, Shin SH, et al: **Perivascular cells induce microglial phagocytic states and synaptic engulfment via SPP1 in mouse models of Alzheimer's disease.** *Nat Neurosci* 2023, **26:**406-415.
40. He Y, Hara H, Nunez G: **Mechanism and Regulation of NLRP3 Inflammasome Activation.** *Trends Biochem Sci* 2016, **41:**1012-1021.
41. Zhou L, Qiu X, Meng Z, Liu T, Chen Z, Zhang P, Kuang H, Pan T, Lu Y, Qi L, et al: **Hepatic danger signaling triggers TREM2(+) macrophage induction and drives steatohepatitis via MS4A7-dependent inflammasome activation.** *Sci Transl Med* 2024, **16:**eadk1866.
42. Lazarov T, Juarez-Carreno S, Cox N, Geissmann F: **Physiology and diseases of tissue-resident macrophages.** *Nature* 2023, **618:**698-707.
43. Park MD, Silvin A, Ginhoux F, Merad M: **Macrophages in health and disease.** *Cell* 2022, **185:**4259-4279.
44. Rizzo G, Gropper J, Piollet M, Vafadarnejad E, Rizakou A, Bandi SR, Arampatzi P, Krammer T, DiFabion N, Dietrich O, et al: **Dynamics of monocyte-derived macrophage diversity in experimental myocardial infarction.** *Cardiovasc Res* 2023, **119:**772-785.
45. Kenkhuis B, Somarakis A, Kleindouwel LRT, van Roon-Mom WMC, Hollt T, van der Weerd L: **Co-expression patterns of microglia markers Iba1, TMEM119 and P2RY12 in Alzheimer's disease.** *Neurobiol Dis* 2022, **167:**105684.
46. Butovsky O, Jedrychowski MP, Moore CS, Cialic R, Lanser AJ, Gabriely G, Koeglsperger T, Dake B, Wu PM, Doykan CE, et al: **Identification of a unique TGF-beta-dependent molecular and functional signature in microglia.** *Nat Neurosci* 2014, **17:**131-143.
47. Dick SA, Wong A, Hamidzada H, Nejat S, Nechanitzky R, Vohra S, Mueller B, Zaman R, Kantores C, Aronoff L, et al: **Three tissue resident macrophage subsets coexist across organs with conserved origins and life cycles.** *Science Immunology* 2022, **7:**eabf7777.
48. Dong L, Hu S, Li X, Pei S, Jin L, Zhang L, Chen X, Min A, Yin M: **SPP1(+) TAM Regulates the Metastatic Colonization of CXCR4(+) Metastasis-Associated Tumor Cells by Remodeling the Lymph Node Microenvironment.** *Adv Sci (Weinh)* 2024, **11:**e2400524.

49. Bill R, Wirapati P, Messemaker M, Roh W, Zitti B, Duval F, Kiss M, Park JC, Saal TM, Hoelzl J, et al: **CXCL9:SPP1 macrophage polarity identifies a network of cellular programs that control human cancers.** *Science* 2023, **381:**515-524.
50. Zhang Y, Zhang L, Xu H, Yin X, Zheng X, Cui N, Lv H, Zhang X, Fang L, Zhang L, et al: **Severe fever with thrombocytopenia syndrome virus infection of the male reproductive tract induces pathology and inflammation.** *Nature Microbiology* 2026.
51. Li B, Liu J, He W, Zhou Y, Zhao M, Xia C, Pan X, Ji Z, Duan R, Lian H, et al: **Inhibition of macrophage inflammasome assembly and pyroptosis with GC-1 ameliorates acute lung injury.** *Theranostics* 2025, **15:**2360-2374.
52. Ma J, Wang Y, Xu W, Wang H, Wan Z, Guo J: **Macrophage pyroptosis in atherosclerosis: therapeutic potential.** *Acta Biochimica Et Biophysica Sinica* 2025, **57:**857-870.
53. Qi M, Gao Z, Qiu Y, Wang R, Tian K, Yue B, Zhang X, Zhang P, Wu Z, Zhu Q, et al: **NOX2 Contributes to High-Frequency Outer Hair Cell Vulnerability in the Cochlea.** *Adv Sci (Weinh)* 2025, **12:**e08830.
54. Ma Q, Wang Q, Zhu Z, Zhou Q, Wang Z, Qian M, Li T, Gu X, Chen Z, Wang X, et al: **Single-Cell Sequencing Reveals Circadian Sensitivity of Noise-Induced Hearing Loss Mediated by Macrophage-Driven NLRP3 Inflammasome Activation.** *Neurosci Bull* 2026, **42:**319-337.
55. Kleinberger G, Yamanishi Y, Suarez-Calvet M, Czirr E, Lohmann E, Cuyvers E, Struyfs H, Pettkus N, Wenninger-Weinzierl A, Mazaheri F, et al: **TREM2 mutations implicated in neurodegeneration impair cell surface transport and phagocytosis.** *Sci Transl Med* 2014, **6:**243ra286.
56. Zhang SS, Zhu L, Peng Y, Zhang L, Chao FL, Jiang L, Xiao Q, Liang X, Tang J, Yang H, et al: **Long-term running exercise improves cognitive function and promotes microglial glucose metabolism and morphological plasticity in the hippocampus of APP/PS1 mice.** *J Neuroinflammation* 2022, **19:**34.
57. Krenkel O, Puengel T, Govaere O, Abdallah AT, Mossanen JC, Kohlhepp M, Liepelt A, Lefebvre E, Luedde T, Hellerbrand C, et al: **Therapeutic inhibition of inflammatory monocyte recruitment reduces steatohepatitis and liver fibrosis.** *Hepatology* 2018, **67:**1270-1283.
58. Zhang Z, Zhang Y, Xia S, Kong Q, Li S, Liu X, Junqueira C, Meza-Sosa KF, Mok TMY, Ansara J, et al: **Gasdermin E suppresses tumour growth by activating anti-tumour immunity.** *Nature* 2020, **579:**415-420.
59. Sanin DE, Ge Y, Marinkovic E, Kabat AM, Castoldi A, Caputa G, Grzes KM, Curtis JD, Thompson EA, Willenborg S, et al: **A common framework of monocyte-derived macrophage activation.** *Science Immunology* 2022, **7:**eabl7482.

Figures

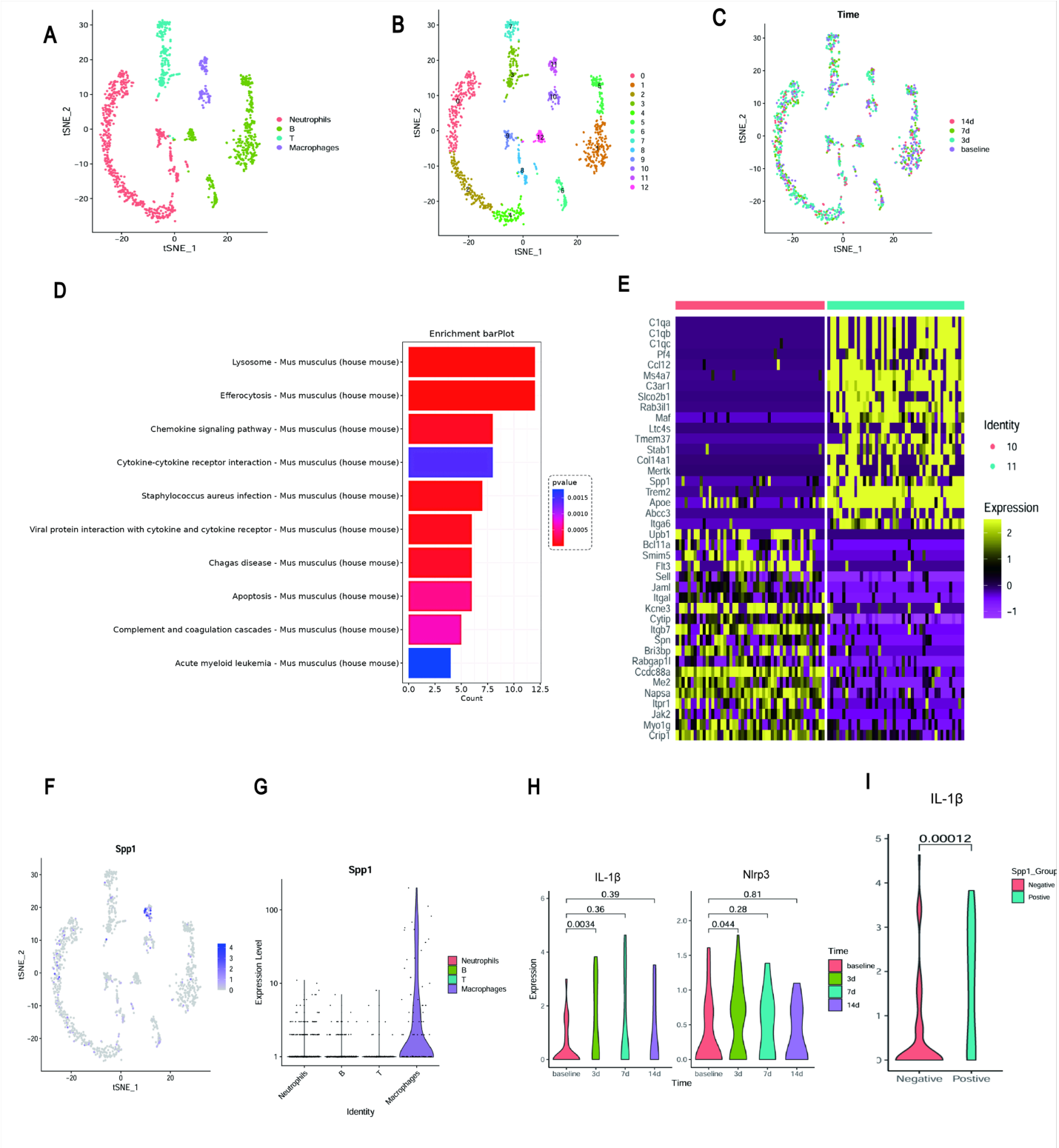


Figure 1

Emergence of an Spp1-highly expressing macrophage subset at three days post-noise exposure. (**A**) t-SNE clustering and cell type annotation of cochlear immune cells, showing major populations including neutrophils, T cells, B cells, and macrophages. (**B**) Clustering dendrogram based on RNA expression similarity, revealing a total of 12 immune cell clusters, with clusters 10 and 11 identified as macrophages. (**C**) Temporal distribution of immune cell clusters across time points. Macrophages at

three days post-noise exposure were predominantly enriched in cluster 11. (**D**) KEGG pathway enrichment analysis of differentially expressed genes in cluster 11 macrophages. (**E**) Heatmap showing differentially expressed genes between clusters 10 and 11. The Spp1-highly expressing macrophage subset exhibited significantly upregulated expression of phagocytosis-related molecules. (**F**) t-SNE plot showing *Spp1* expression distribution. (**G**) *Spp1* expression was specifically elevated in macrophages. (**H**) Expression levels of the inflammasome components *Nlrp3* and *Il1b* were significantly increased in macrophages following noise exposure. (**I**) IL-1β expression levels differed significantly between $Spp1^{+}$ and $Spp1^{-}$ macrophages.

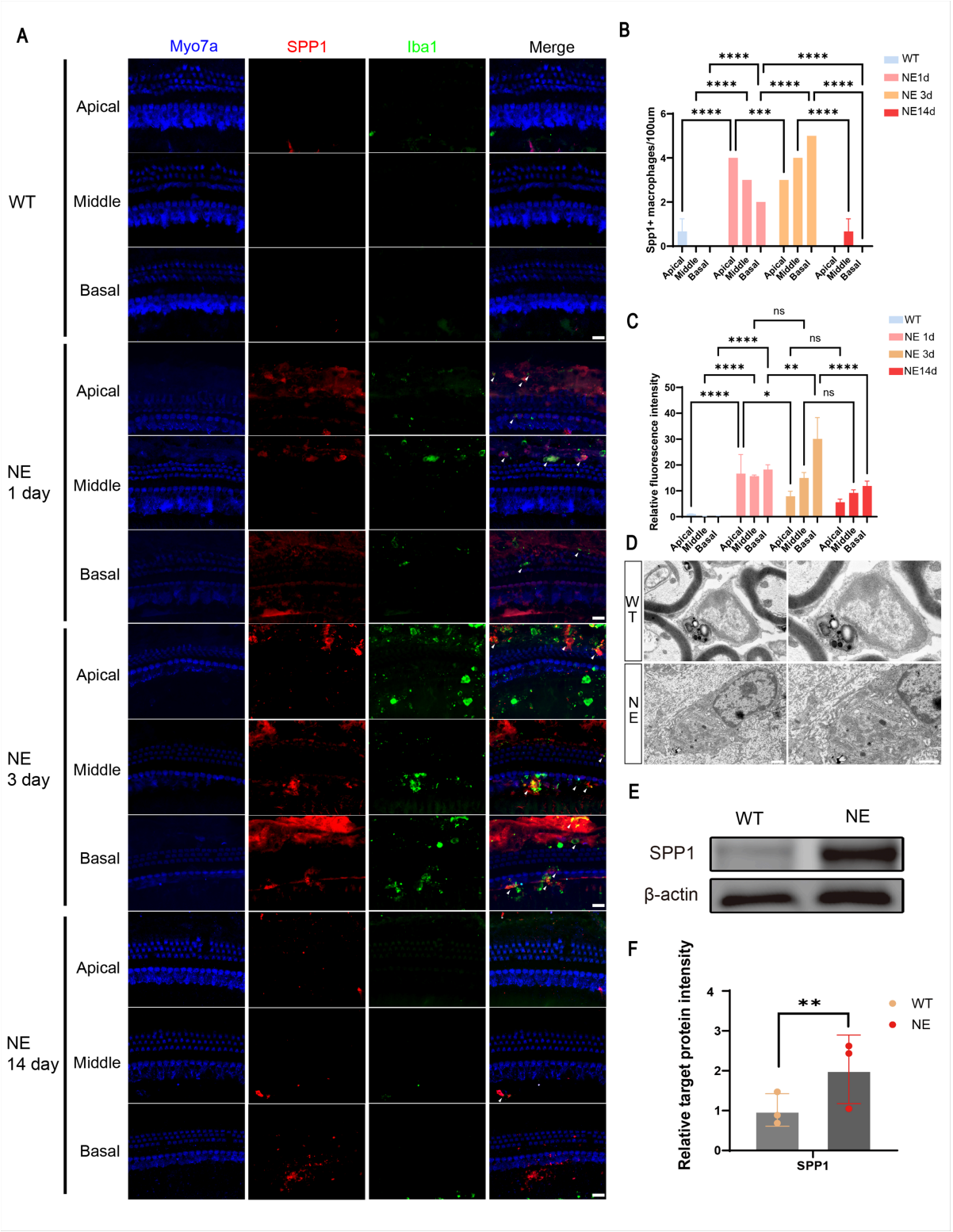


Figure 2

SPP1^{+} macrophages increases after noise exposure.

(**A**) Immunofluorescence staining of cochlear basilar membrane whole mounts before noise exposure and at 1 day, 3 days, and 14 days post-noise exposure, showing SPP1 (red), Iba1 (macrophage marker), and Myo7a (hair cell marker). Representative images. (**B**) Quantification of SPP1-highly expressing macrophages from the images shown in (A)(n=3). (**C**) Quantitative analysis of relative SPP1

fluorescence intensity from the images shown in (A)(n=3). (**D**) Transmission electron microscopy images of cochlear macrophages before noise exposure and at 3 days post-noise exposure. (**E–F**) Western blot analysis showing elevated SPP1 protein levels in the mouse cochlea at 3 days post-noise exposure. ns, not significant; * $p<0.05$; ** $p<0.01$; *** $p<0.001$; **** $p<0.0001$.

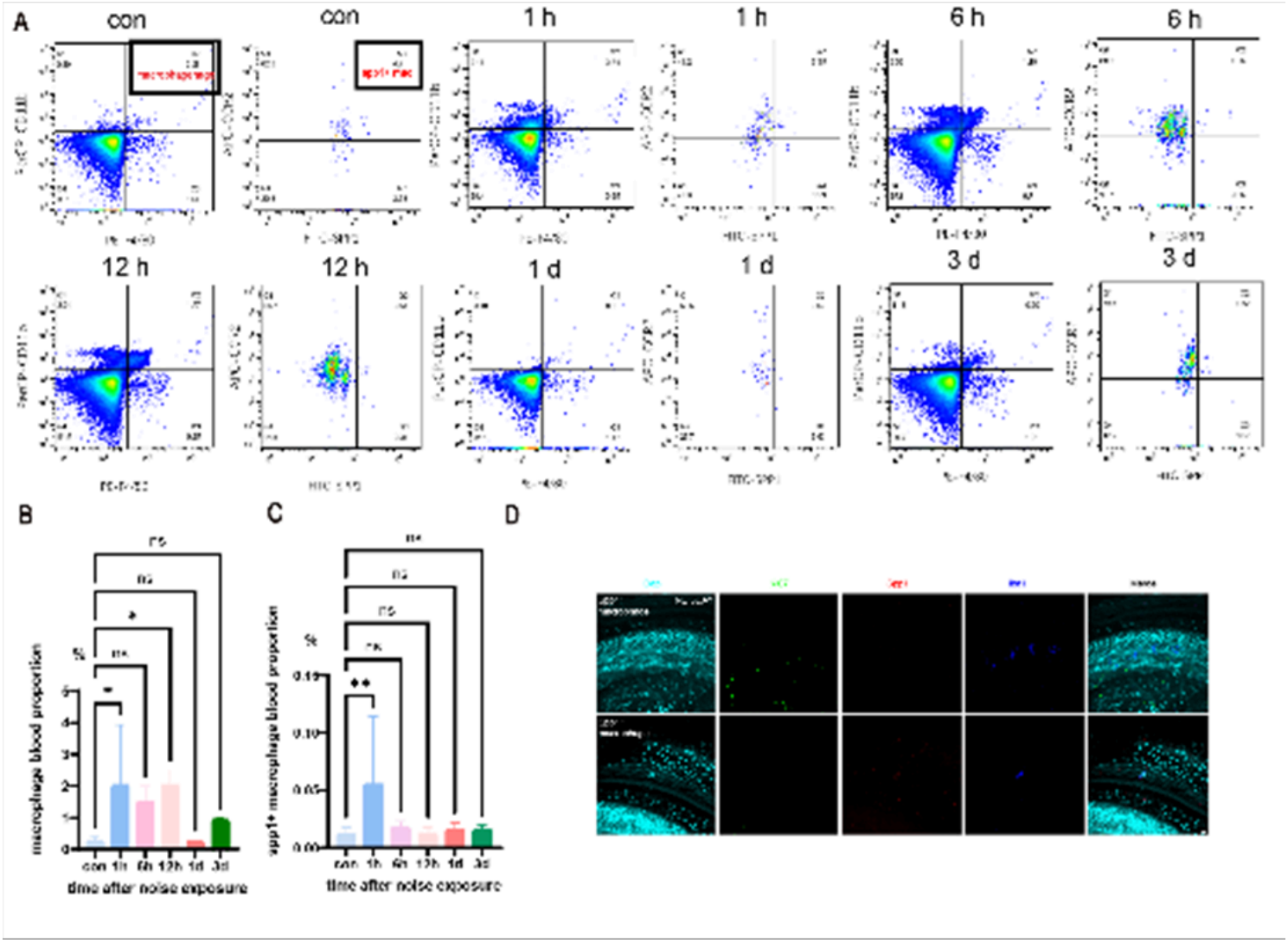


Figure 3

CCR2 signaling mediates the increase of SPP1⁺ macrophages after noise exposure.
(**A**) Flow cytometric quantification of blood macrophages (CD11b⁺ F4/80⁺) and SPP1⁺ macrophages (CD11b⁺ F4/80⁺ CCR2⁺ SPP1⁺) in C57BL/6 mice before noise exposure and at 1 h, 6 h, 12 h, 1 d, and 3 d post-noise exposure. (n = 3) from three independent experiments. (**B**) Quantitative analysis of blood macrophages from the data shown in (A). (**C**) Quantitative analysis of blood SPP1⁺ macrophages from the data shown in (A). ns, not significant; * $p<0.05$; ** $p<0.01$.

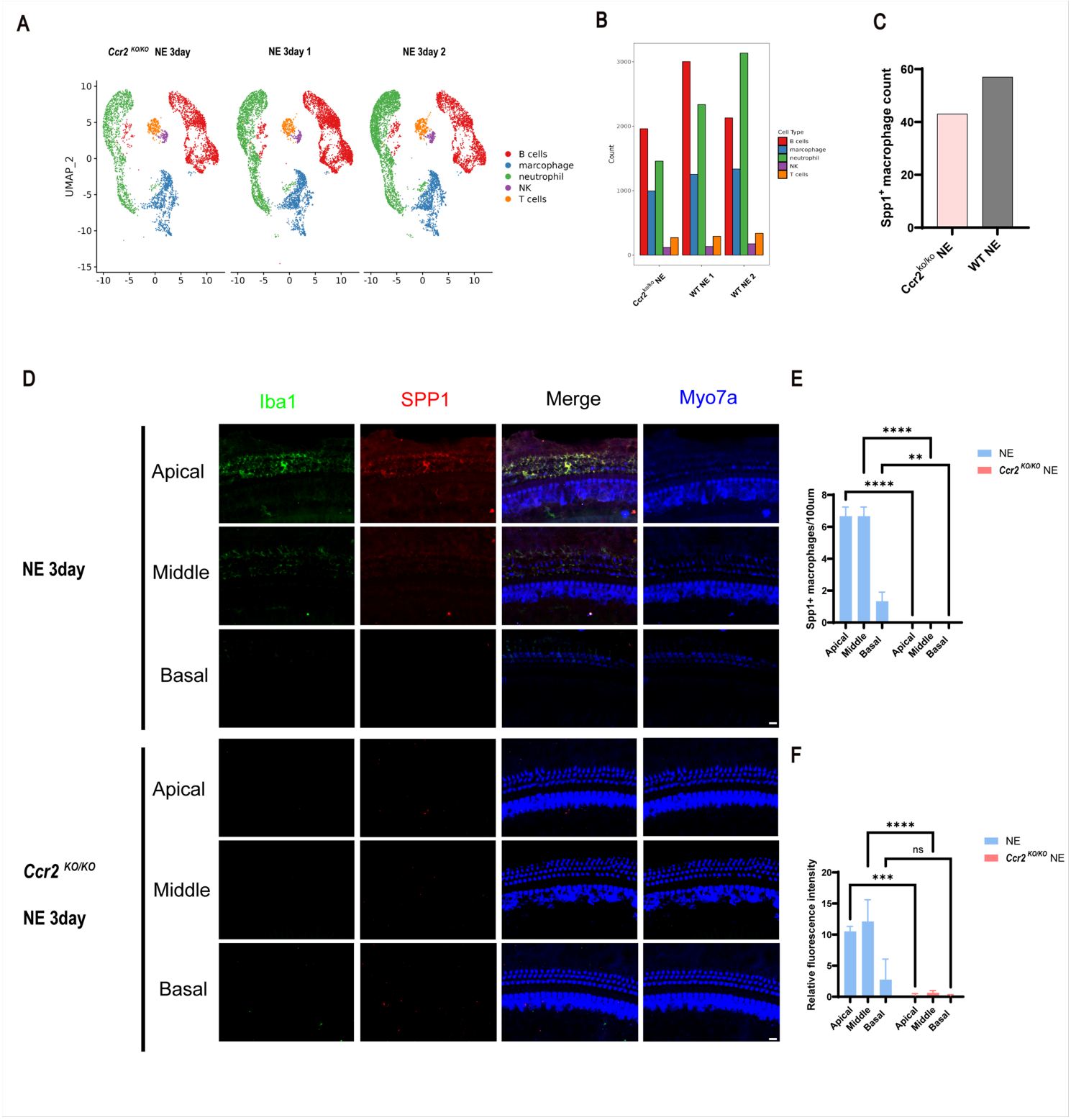


Figure 4

CCR2 knockout leads to a reduction in SPP1⁺ macrophages recruited after noise exposure
(**A**) t-SNE clustering and cell type annotation of cochlear immune cells, showing major populations including neutrophils, T cells, B cells, macrophages, and NK cells**B)** Bar plot illustrating the cellular composition of cochlear immune populations in noise-exposed Ccr2$^{KO/KO}$ mice and two independent noise-exposed wild-type groups.(**C**) Quantification of SPP1⁺ macrophage abundance in the cochlea of

Ccr2 KO/KO and wild-type mice at 3 days post-noise exposure. CCR2 knockout leads to a decrease in the number of macrophages and neutrophils .(**D**) Immunofluorescence staining of Iba1, SPP1, and Myo7a in the apical, middle, and basal turns of the cochlea at 3 days post-noise exposure in WT and $Ccr2^{KO/KO}$ mice.(**E**) Quantification of $SPP1^{+}$ macrophage density (cells per 100 μm) in the apical, middle, and basal turns of wild-type and $Ccr2^{KO/KO}$ mice at 3 days post-noise exposure.(n=4)(**F**) Relative fluorescence intensity of SPP1 in the apical, middle, and basal turns of $Ccr2^{KO/KO}$ mice at 3 days post-noise exposure. (n=4)ns, not significant; ** p<0.01; *** p<0.001; **** p<0.0001

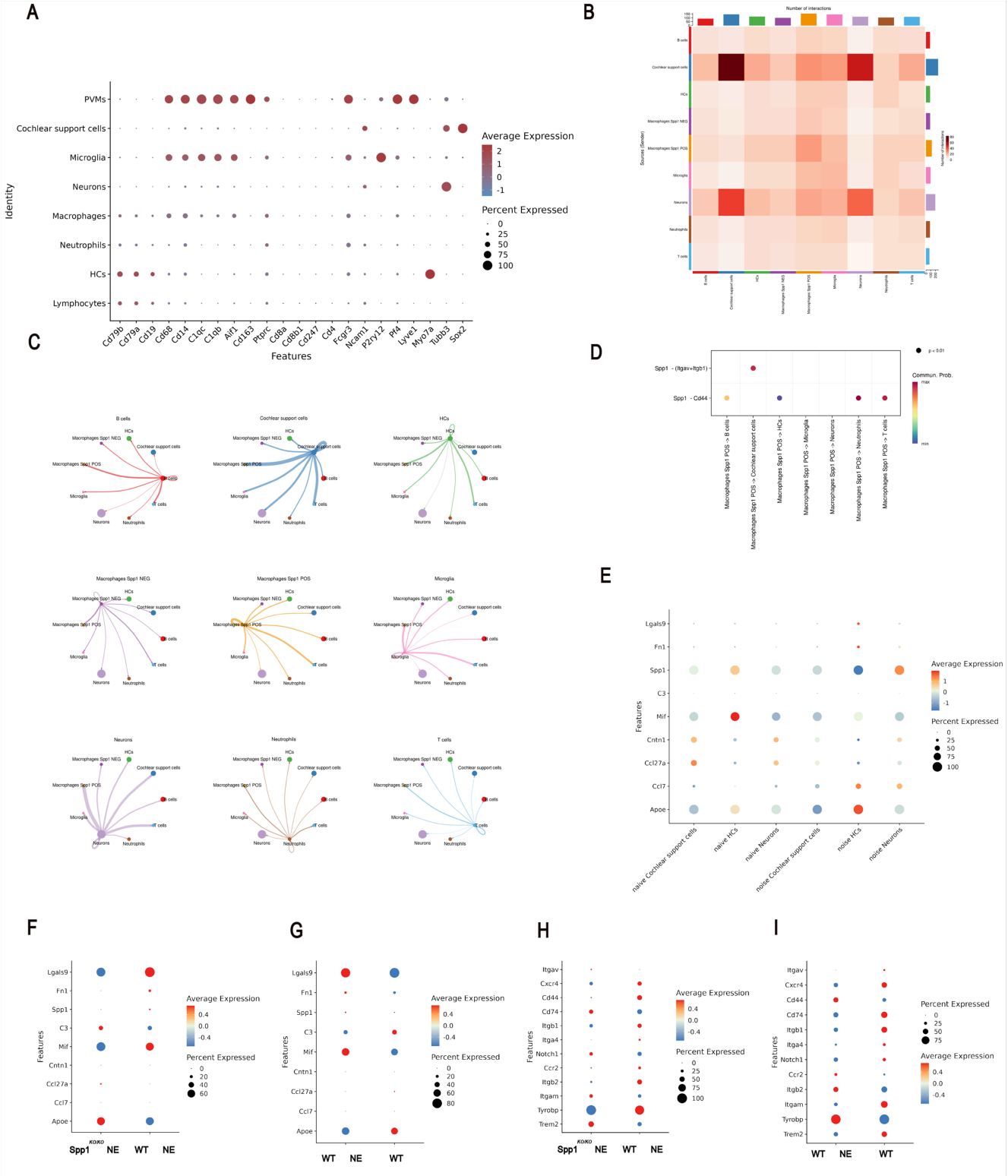


Figure 5

spp1 mediates communication and pro-inflammatory responses between macrophages and other cells
(**A**) Dot plot showing marker gene expression for annotated cochlear cell types. (**B**) Heatmap depicting the overall cell–cell communication network among cochlear cell types. SPP1^{+} macrophages displayed the most frequent intercellular communications. (**C**) Chord diagram illustrating that SPP1^{+} macrophages exhibit the most extensive i01nteractions with nearly all other cochlear cell types□B cells □T cells□

macrophages□Neutrophils□Cochlear support cells□HCs□Neurons□. (**D**) Dot plot showing ligand–receptor interactions between SPP1⁺ macrophages and other cochlear cell types. SPP1^{+} macrophages establish close communication with cochlear supporting cells through (SPP1-itgav+itgb1). In addition, SPP1⁺ macrophages form close interactions with neutrophils, T cells and B cells through (SPP1-CD44). (**E**) Changes in ligand expression in cochlear supporting cells, hair cells, and neurons before and after noise exposure. (**F**) Dot plot showing alterations in ligand expression levels in macrophages upon *Spp1* knockout. (**G**) Ligand expression levels in macrophages before and after noise exposure. (**H**) Dot plot showing alterations in receptor expression levels in macrophages upon *Spp1* knockout. (**I**) Receptor expression levels in macrophages before and after noise exposure.

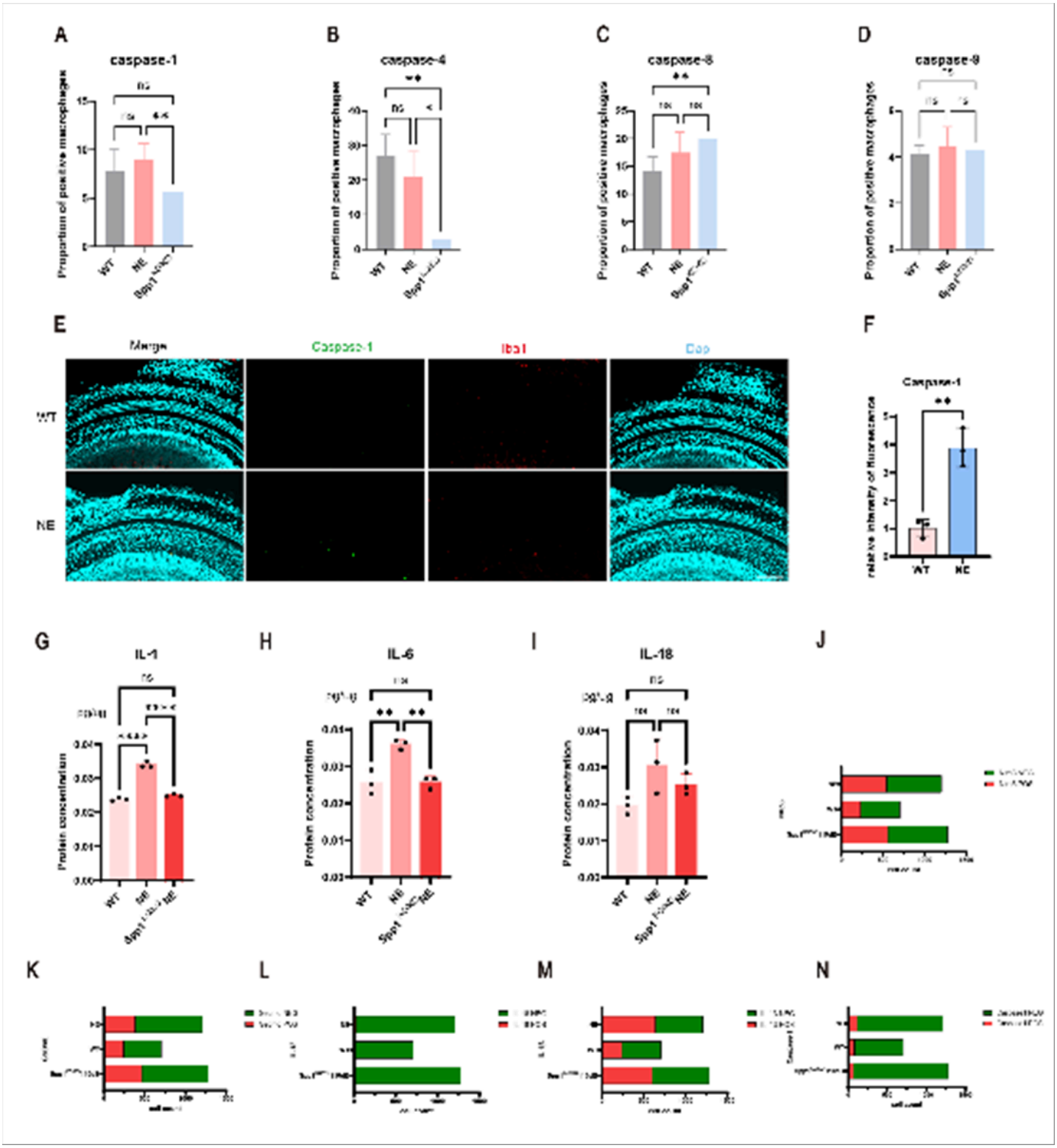


Figure 6

Knockout of spp1 leads to the blockade of the noise-induced caspase-1-mediated pyroptosis pathway in macrophages.

(**A–D**) Proportions of macrophages expressing pyroptosis-related molecules caspase-1, caspase-4 and apoptosis-related molecules caspase-8, caspase-9 in single-cell sequencing; the proportion of macrophages expressing pyroptosis-related molecules was significantly decreased after spp1 knockout.

(**E-I**) Contingency table showing the proportion of macrophages expressing pyroptosis-related molecules(Nlrp3、GSDMD、caspase-1、IL-18、IL-1β). (**J-L**) Expression levels of IL-1β, IL-6, and IL-18 in the cochlea of wild-type mice before and after noise exposure, and in *Spp1* $^{KO/KO}$ mice at 3 days post-noise exposure. ns, not significant; ** p<0.01; **** p<0.0001.

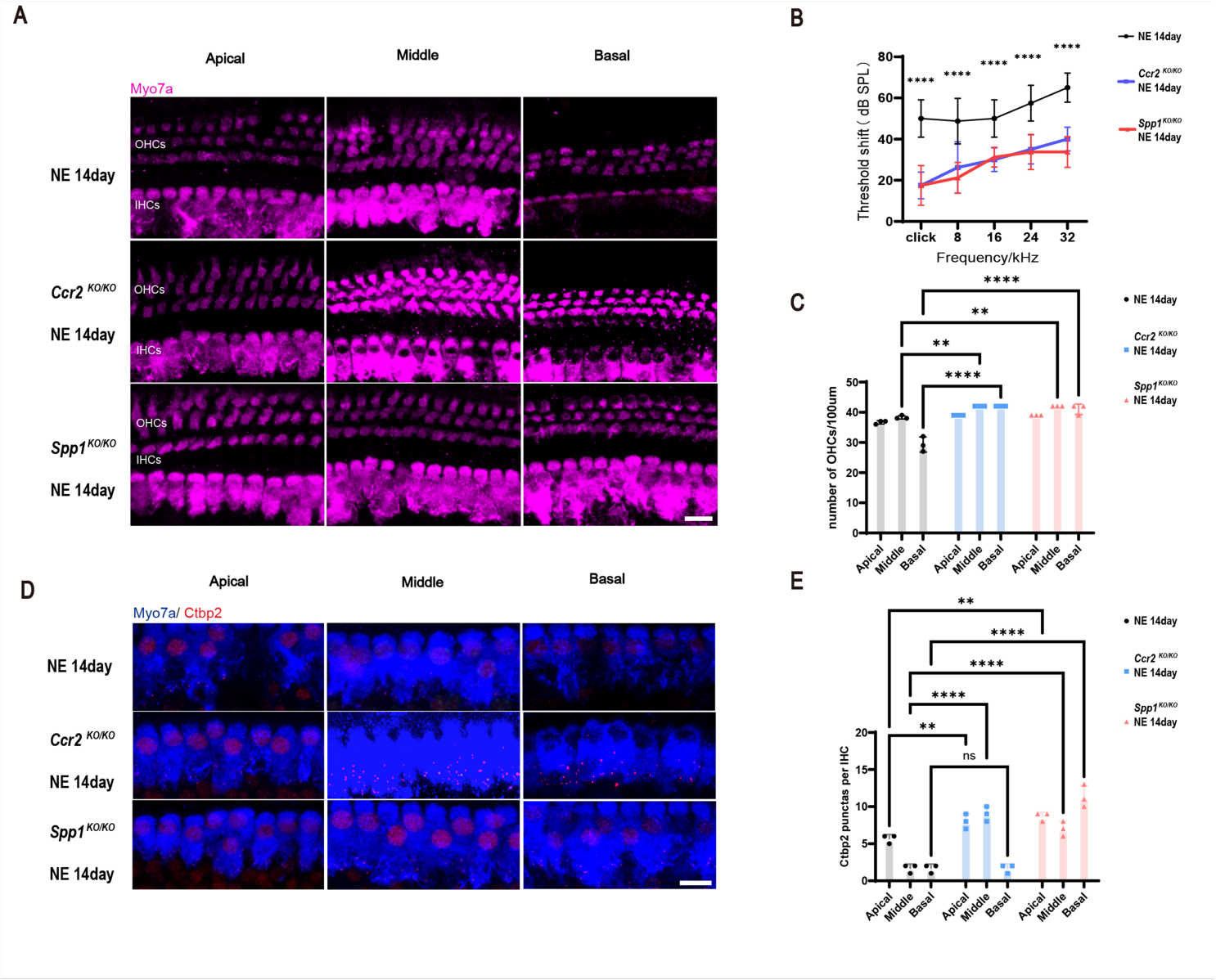


Figure 7

Protective effects of *Ccr2* and *Spp1* knockout against noise-induced hearing loss.
(**A**) Immunofluorescence staining of cochlear hair cells (Myo7a) in the apical, middle, and basal turns of wild-type mice, *Ccr2* $^{KO/KO}$ mice, and *Spp1* $^{KO/KO}$ mice at 14 days post-noise exposure. (**B**) Auditory brainstem response (ABR) threshold shifts in mice at 1 day and 14 days after noise exposure. (n=6) (**C**) Quantification of hair cell counts from the images shown in (A). (n=3) (**D**) Immunofluorescence staining of inner hair cells (Myo7a) and synapses (CtBP2) in the apical, middle, and basal turns of wild-type

mice, *Ccr2* $^{KO/KO}$ mice, and *Spp1* $^{KO/KO}$ mice at 14 days post-noise exposure. (**E**) Quantification of synapse counts from the images shown in (D). (n=3) ns, not significant; ** p<0.01; **** p<0.0001.

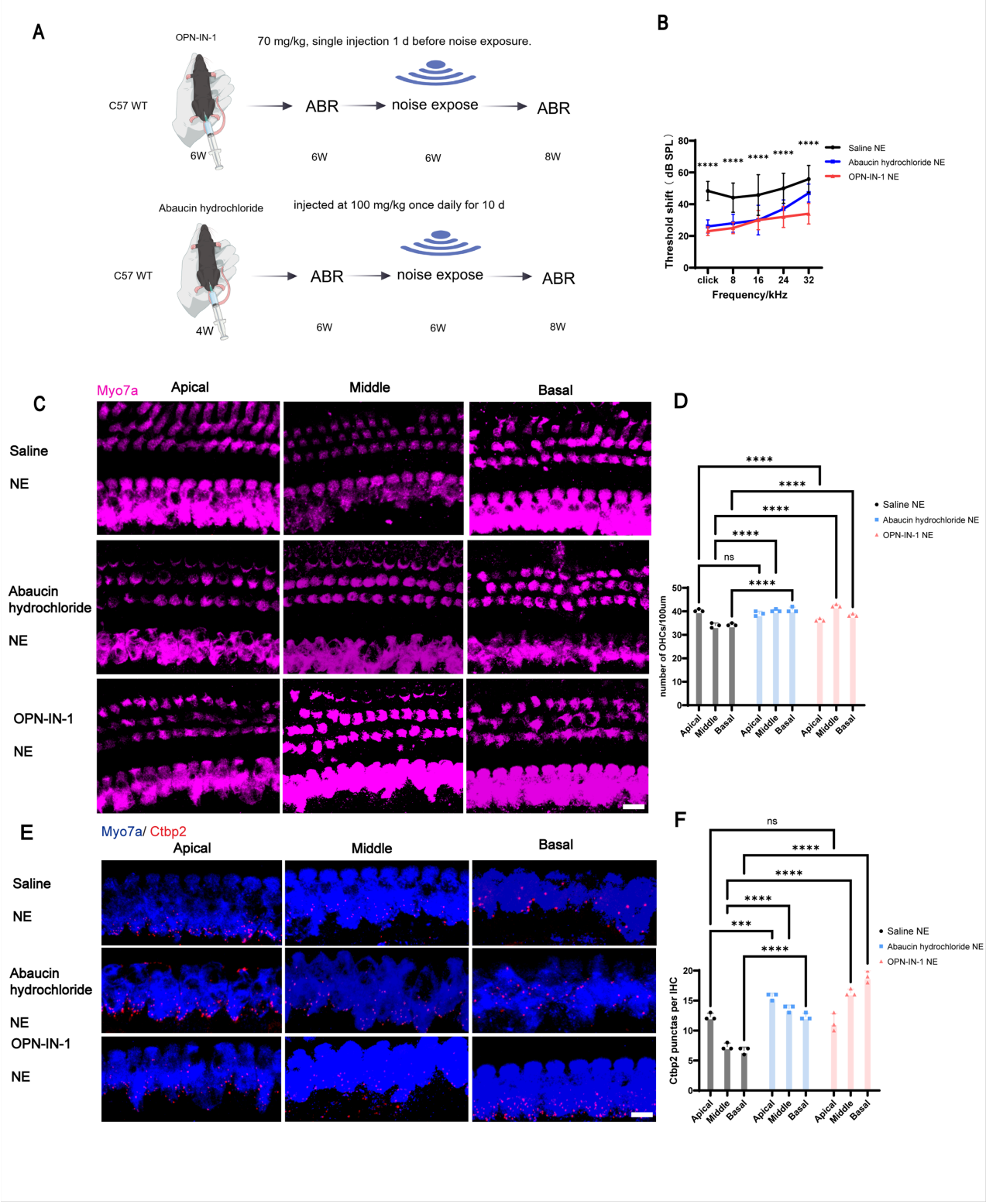


Figure 8

Hair cell and synapse staining and auditory threshold shifts after noise exposure following administration of SPP1 and CCR2 inhibitors.

(**A**) Dosing regimen and administration schedule of SPP1 inhibitor and CCR2 inhibitor.
(**B**) Auditory brainstem response (ABR) threshold shifts in mice at 1 day and 14 days after noise exposure. (n=6)(**C)** Immunofluorescence staining of cochlear hair cells (Myo7a) in the apical, middle, and basal turns of wild-type mice before and after noise exposure.(**D**) Quantification of hair cell counts from the images shown in (C). (n=3) (**E**) Immunofluorescence staining of inner hair cells (Myo7a) and synapses (CtBP2) in the apical, middle, and basal turns of wild-type mice before and after noise exposure. (**F**) Quantification of synapse counts from the images shown in (E). (n=3) ns, not significant; *** $p<0.001$; **** $p<0.0001$.

Supplementary Files

This is a list of supplementary files associated with this preprint. Click to download.

- S1.tif
- S2.tif
- S3.tif
- S4.tif